Design of MTM-Based Multiband Micro-Biosensor in Terahertz Region as Perfect Absorber for Early-Stage Leukemia Diagnosis With Sensitivity 18 626 373 THz/RIU

Musa N. Hamza and Mohammad Tariqul Islam, *Senior Member, IEEE*

***Abstract*—In this article, a novel highly sensitive biosensor based on perfect metamaterial (MTM) absorbers is presented. A detailed study is presented for several different models, different types of substrate materials, different types of resonant materials, and substrate thicknesses showing very good sensitivity to any changes. The proposed biosensor exhibits high sensitivity to different polarization and incidence angles, ensuring its performance in terms of signal-to-noise ratio (SNR). The proposed biosensor was carefully compared with previously designed sensors and biosensors. The proposed biosensor exhibits amazing sensitivity, such as a quality factor (*Q*-factor) of 41.1, a figure of merit (FOM) of 172 466 416 RIU^{-1}, and a sensitivity (*S*) of 18 626 373 THz/RIU. The high sensitivity of the biosensor allows early detection of leukemia, demonstrating significant differences between leukemia and normal blood. Another interesting result of this article is the use of terahertz (THz) waves for imaging. Microwave imaging (MWI) is performed for electric fields, magnetic fields, and power.**

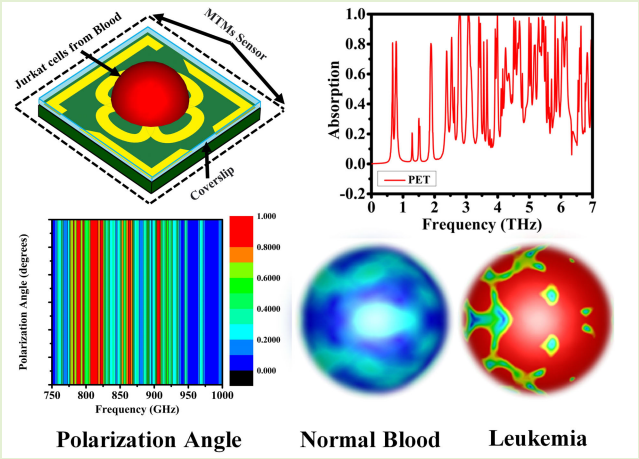

***Index Terms*— Biosensor, blood cancer, Jurkat cell, leukemia, metamaterial perfect absorbers (MTMPAs), multiband in THz, MWI technique.**

I. Introduction

CANCER is among the worst diseases that humans have ever encountered. An estimated 17 million people will die from cancer-related causes, and 26 million new cases of cancer will be diagnosed by 2030 [1]. Blood malignancies, known as leukemias [2], are considered aggressive diseases. Because this condition is linked to white blood cells (WBCs) or leukocytes, it has the potential to harm the human body, particularly the blood and bone marrow. The prevalence of blood cancers is increasing annually due to genetic and environmental factors [3]. Acute leukemias are categorized into two main classes: myeloid and lymphoid [4], with acute lymphocytic leukemia (ALL) being the most common in children and acute myeloid leukemia (AML) being the most common in adults [2], [5]. Their incidence and mortality rates rank 15th and 10th for all malignant cases, respectively [6], [7]. ALL is a lethal illness characterized by the transformation and proliferation of lymphoid progenitor cells in the bone marrow, blood, and extramedullary locations. It affects 1.6 per 100 000 people in the U.S. [8], with over 1400 deaths in 2016 [9]. The illness has a bimodal distribution, with a first peak in youth and a second peak around the age of 50 [10]. Although dose-intensification methods have improved results for pediatric patients, the elderly continue to have a dismal prognosis. Only 30%–40% of adult patients with ALL achieve long-term remission [11]. Early detection of ALL is essential for recovery, especially in children. However,

Manuscript received 24 February 2024; revised 24 March 2024; accepted 27 March 2024. Date of publication 8 April 2024; date of current version 15 May 2024. This work was supported by the Fundamental Research Grant Scheme (FRGS) funded by the Ministry of Higher Education (MOHE), Malaysia, under Grant FRGS/1/2021/TK0/UKM/01/6. The associate editor coordinating the review of this article and approving it for publication was Prof. Mohammad Hossein Zarifi. *(Corresponding author: Mohammad Tariqul Islam.)*

Musa N. Hamza is with the Department of Physics, College of Science, University of Raparin, Sulaymaniyah 46012, Iraq (e-mail: musa.nuraden@uor.edu.krd).

Mohammad Tariqul Islam is with the Department of Electrical, Electronic and Systems Engineering, Faculty of Engineering and Built Environment, Universiti Kebangsaan Malaysia (UKM), Bangi 43600, Malaysia (e-mail: tariqul@ukm.edu.my).

Digital Object Identifier 10.1109/JSEN.2024.3383522

the similarities between normal and lymphoid cell types make this difficult. Accurate diagnosis requires manual analysis of bone marrow samples, which is time-consuming and subject to expert judgment. The pathologist's expertise is essential, but human error can still occur. Therefore, an early diagnosis is essential for a good recovery [12].

Terahertz (THz) waves are waves that span the infrared and microwave wavelengths [13]. Because of their unique properties, including fingerprint spectroscopy, non-ionization, high penetration, low photon energy, and molecular signatures, these waves are well-suited for sensing applications in a variety of industries, including biology, telecommunications, security, and medicine. THz waves may detect weak resonance between molecules, which is not detectable by conventional mid-infrared spectroscopy. This creates new opportunities for methods of separating biomolecules and detecting matter [14]. THz waves are well suited for security imaging and identification of biological objects due to their ability to transmit through non-polar materials and exhibit optical transparency [15], [16], [17], [18], [19]. On the other hand, the long wavelength of THz radiation leads to poor spatial resolution and poor accuracy when measuring materials with dimensions significantly smaller than the micrometer scale. Metamaterials (MTMs) consisting of subwavelength periodic metallic structures or dielectric structures (meta-atoms) can increase THz detection sensitivity and achieve subwavelength spatial resolution to overcome this limitation. THz sensing involves detecting a change in the absorption peak in the spectrum caused by the presence of an analyte, as well as a change in the resonant frequency of THz devices produced by the increase in refractive index (RI) around the metasurface. MTMs can help sensors detect and amplify small changes caused by weak interactions of analytes with electromagnetic (EM) stimuli [20], [21]. Due to their ability to alter the rules of optics and EMs [22], MTMs have a wide range of applications in biosensing, imaging, antenna engineering [23], [24], [25], [26], [27], and optoelectronics [28]. THz offers wide bandwidth, little scattering, and non-ionizing features in MTM-based perfect absorbers (MTMPAs). These absorbers use dielectric layers, metallic patterns, and continuous metallic layers. High-ε materials reduce the dielectric layer thickness while maintaining the optical path for EM waves. The resonant frequency, which encompasses both single and multiresonance modes of THz metasurfaces, is used to illustrate the sensitivity of THz sensors. THz is a special spectrum of frequencies that may be employed in MTMPAs to analyze biological or chemical materials at the nanoscale with the purpose of characterizing their structural behavior. These absorbers consist of dielectric layers, continuous metallic layers, and metallic patterns. High-ε materials thin the dielectric layer while preserving the EM waves' optical path. By monitoring the shift in the resonance-band absorption peak, the sensors are able to identify variations in the RI of the medium. THz sensing entails monitoring the shift in the absorption peak produced by the presence of the analyte, as well as the resonant frequency shift from THz devices generated by the changing ambient RI surrounding the metasurface. The resonant frequency, which encompasses single and multiresonance modes of THz metasurfaces, is used to demonstrate the sensors' sensitivity. The inherent resonance frequencies of THz metasurfaces are determined by the different geometry of meta-atoms.

Perfect MTM sorbents show significant advantages over conventional sorbents in the context of biosensing, especially leukemia detection. These engineered structures leverage precise THz resonance to meticulously match the vibrational signatures of target biomolecules, delivering spectral specificity superior to the absorption broadband of traditional absorbers. This targeted approach improves sensitivity and specificity, enabling accurate, label-free detection with minimal interference from other biological components. The label-free nature of the MTM sorbent, eliminating the need for fluorescent or radioisotope labels, supports real-time, noninvasive analysis that is beneficial for rapid diagnosis. The micrometer-scale size of these sorbents allows for miniaturization, facilitating the development of portable and cost-effective biosensing devices suitable for healthcare environments. Integration with a microfluidic platform enables continuous flow analysis and automation, streamlining the diagnostic process. In addition to these features, dynamic control through external stimuli, such as temperature or voltage, provides adaptability to meet different sensing needs. Additionally, the hybridization of MTMs with other sensing components will create multifunctional platforms with amplified performance. Unlike conventional absorbers, including blackbodies, semiconductor-based and organic alternatives, MTM absorbers have outstanding selectivity, durability, and adaptability. This combination of high sensitivity, label-free sensing, miniaturization, and tunability positions MTM absorbers as promising contenders for personalized medicine and early disease detection, especially in diagnosing leukemia. Ongoing research and development are expected to refine these capabilities, translating the potential of MTM biosensing into tangible medical breakthroughs.

In this article, a unique highly sensitive biosensor based on perfect MTM absorbers (PMAs) is presented. An in-depth study is provided for a variety of designs, substrate types, resonator materials, and substrate thicknesses, demonstrating very good sensitivity to any changes. The proposed biosensor exhibits high sensitivity at different polarization and incidence angles, ensuring excellent signal-to-noise ratio (SNR) performance. The proposed biosensor was thoroughly compared with previously designed sensors and biosensors. The high sensitivity of the biosensor allows early identification of leukemia, showing significant differences between leukemia and normal blood. THz wave imaging is another intriguing outcome of this article. Microwave imaging (MWI) is performed for electric fields, magnetic fields, and power.

II. Literature Review

MTMs have been used in the past to build a variety of sensors for a range of purposes, such as: Al-Naib et al. [29] introduced asymmetric single ASRs in a mirrored arrangement that dramatically increases the quality factor (Q-factor) of the inductive-capacitive resonance. Park et al. [30] employed the single split-ring resonator (SRR) to detect fungi and bacteria.

Zhang et al. [31] presented a PIT MTM that is not reliant on polarization. Hu et al. [32] studied THz SRR transmission responses in different polarization orientations to determine petrol. Li et al. [33] developed an all-dielectric EIT-like MTM that is polarization-insensitive. Xie et al. [34] described their use of THz biosensors for antibiotic detection. Guo and Argyropoulos [35] introduced THz metasurfaces using aligned graphene patches for polarization conversion. Park et al. [36] used a nanogap-metasurface-based THz sensor to detect viruses. Vafapour and Forouzeshfard [37] demonstrated the disappearance of plasmonically induced reflectance in MTMs by breaking symmetry in both I-II and H-II structures, proving the possibility of creating PIR effects in symmetric structures. Shukla et al. [38] introduced a biosensor for sequencing DNA. Graphene and hexagonal boron nitride nanogaps are used in the biosensor [38].

Ma et al. [39] suggested a silicon-based MTM that exhibits an EIT-like effect at THz frequencies. In biomedicine, EIT-like sensors are frequently employed in the THz region. Yan et al. [40] presented a biosensor that resembles a THz EIT. The sensor was loaded with HSC3 oral cancer cells [40]. Nevertheless, lithography technology poses manufacturing hurdles for real-world applications of nanogap sensors [41]. With the recent advancement of atomic layer deposition (ALD) technology [42], the challenge has been solved and nanogaps smaller than 1 nm wide may now be produced [56]. Chen et al. [43] introduced a structure made up of four SRRs and a Cross (FSRRC) that spins the SRR in the direction of the middle gap. Furthermore, when the symmetrical structure was swapped to the asymmetrical one, Fano resonance was generated [44], boosting the sensitivity of the system and producing two additional resonant peaks.

Chen et al. [45] made nanoscale structural modifications to the FSRRC to detect transmission. It is ideal for accurately recognizing small illnesses, like viruses, because of its two frequency characteristics [45]. A quad-band plasmonic perfect absorber (PPA) based on an all-metal nanostructure metasurface in the infrared regime was suggested and quantitatively studied by Zhang et al. [46]. This device has potential applications in RI sensing [46]. Zhang et al. [47] proposed a biosensor with an EIT-like structure to classify and detect chemicals associated with glioma cells. Vafapour et al. [48] present a new superconducting PrMM class, with potential applications in temperature sensors, thermo-optical modulators, and magnetic switch devices.

Hamouleh-Alipour et al. [49] introduced a label-free biosensor using surface plasmon resonances for measuring blood Hb concentration, potentially being a dual-bands metasurface perfect absorber (PA). Vafapour [50] study explores a THz-absorbing-metasurface BEA-style design using low-cost materials and the Drude model for semiconductor dielectric function, describing both free-electron and bound systems. Karki et al. [51] developed a surface plasmon resonance-based biosensor for cancer cell detection, improving sensitivity and performance across various RI variations. A dual-band THz PA based on an all-dielectric MTM made of the InSb array's vertical-square-split-ring (VSSR) structure was suggested and numerically studied by Li et al. [52]. Xu et al. [53] introduced a spoof LSP structure in the THz frequency. By using the bright broadband dipole mode to cover several dark spoof LSP modes, three induced transparent peaks are created [53]. Wang et al. [54] introduced a dual-parameter sensing approach using SPR-PCF with two open ring channels. The sensor, coated with gold and silver layers and filled with MF and PDMS, detects magnetic field and temperature. Finite element method analysis examines its mode characteristics, structure parameters, and sensing performance [54]. Shangguan et al. [55] introduced a highly sensitive active adjustable graphene absorber for RI sensing. Their proposed three-band absorber, Au-SiO_2-Graphene, demonstrates superior physical mechanisms. Active adjustability is achieved by regulating the Fermi level of graphene, enhancing its potential for sensing applications [55].

Saxena et al. [56] introduced a multiband THz MIMO antenna, $80 \times 100 \times 10.8\ \mu m^3$, on a gold-plated Arlon AD410 substrate for biomedical sensing. Ji et al. [57] presented an extremely sensitive method for detecting viruses using gold nanogaps that included Al_2O_3. Later, in a book Yadav and Gorodetsky [58] focused on the various applications of THz, especially for the early detection of different cancer cells and the use of THz for biological imaging. In another part of the same book, Rafailov and Gric [59] focus on various applications of THz, especially in the treatment of various cancer cells and the development of artificial intelligence-based biosensors. Almawgani et al. [60] developed a highly sensitive surface plasmon resonance sensor for blood cancer detection, demonstrating the potential of early discovery in increasing treatment success. Elhelw et al. [61] proposed and quantitatively analyzed a highly sensitive triple-band MTM-based biosensor for detecting various cancer cells. Cheng et al. [62] introduced two types of waveform-selective microwave metasurface absorbers (MMAs) with a single square-patch structure and a lumped nonlinear circuit. These MMAs were designed to preferentially absorb signals at the same frequencies, including a higher-order mode [62].

A micro-ring-shaped structure-based narrowband perfect metasurface absorber (MSA) was introduced by Cheng et al. [63]. A GaAs array was suggested and theoretically studied in the THz range, with potential applications in increased RI sensing [63]. Three-row metasurface units within a group independently interact with three pairs of orthogonal polarization channels in Huang et al. [64] introduction and proposal of an interleaved meta-lens arrangement for polarization imaging. Ma et al. [65] introduced a highly sensitive, multiadjustable five-peak graphene absorber for far infrared applications. Their proposed absorber comprises a traditional MPA structure with a graphene array embedded with four-angle star patterns. Plasmon resonance on the graphene surface in the incident far-infrared wave was studied, enhancing sensing capabilities. Zhu et al. [66] introduced a PCF plasmonic sensor with a U-shaped channel, aiming to enhance optical fiber sensing. They explored structural parameters' influence and mode characteristics using COMSOL and coupled mode theory [66]. Hamza and

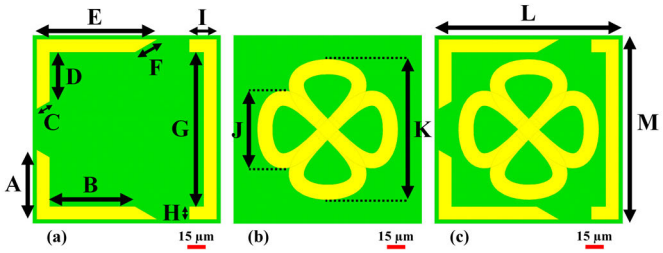

Fig. 1. Structural design of the proposed PA (a) first resonators, (b) second resonators, and (c) proposed design.

TABLE I
COMPLETE LIST OF THE VARIABLES THAT HAVE BEEN ADJUSTED FOR THE RECOMMENDED SENSOR

Parameter	Value (µm)	Parameter	Value (µm)
A	55.5	H	10.3
B	68.1	I	21.8
C	11.8	J	62
D	39.3	K	112
E	96.1	L	150
F	20.5	M	150
G	123		

Islam [67] our previous work, a novel THz biosensor was developed using MTMs for perfect absorption, allowing for the development of a tiny dual-band biosensor for non-melanoma skin cancer diagnostics.

III. MODEL'S UNIT CELL LAYOUT

The biosensor's sensitivity, specificity, and selectivity will all be considered in the design. These elements play a part in the precise and trustworthy diagnosis of blood cancer. The requirement for high sensitivity and specificity limits and complicates the design of biosensors used for this purpose. Notwithstanding these difficulties, biosensor performance has to be improved in order to enhance clinical efficacy and offer valuable data for blood cancer detection. Combining the second model, shown in Fig. 1(a), with the fifth model, shown in Fig. 1(b), results in a perfectly absorbing MTM proposed as a sensor, as shown in Fig. 1(c). This combination has been used to construct multiband THz oscillators. The proposed system consists of three layers, each with a dielectric in the middle and a full electrical conductor on both sides. The purpose of merging the shapes is to overcome the magnetic and electric forces that pass through and interact with them. Table I summarizes the instructional data from the models. Large-scale integration (LSI) is recommended based on computer-aided design (CAD). The properties of MTM can be verified, and the behavior of MTM quality at different frequency and size ranges can be expressed by quantitative calculations. Scientists have used numerical analysis to study a variety of designs, including unit cells, free space, periodic lattices, and perfect electrical and magnetic conductors (PEC and PMC). A unit cell is specified in the x- and y-direction, and an additional open space is specified in the z-direction to streamline simulation procedures. The model's three-layer design includes an aluminum (Al) upper and lower layer and a polyethylene terephthalate (PET) dielectric pad in the middle layer. Below are some properties of aluminum (Al): 23e-6 K^{-1}, 3.56e + 07 $S.m^{-1}$, 237 $W.m^{-1}K^{-1}$, 0.9 $kJ.K^{-1}.kg^{-1}$, 9.75309e-05 $m^2.s^{-1}$, 0.33, 69 $kN.mm^{-2}$, and 2700 $kg.m^{-3}$. which include thermal expansion, electrical conductivity (σ), thermal conductivity (k), specific heat capacity (Cs), diffusivity, Poisson's ratio, Young's modulus, and density, respectively. The dielectric spacer was 10 μm thick, and the conductivity of aluminum (Al) was 3.56×10^7 S/m. The thickness of the top and bottom aluminum (Al) layers is 0.2 μm. To allow the maximum amount of energy to penetrate and transmit through PET, the top metal layer has been designed to match its impedance to that of the incident medium. The purpose of the bottom aluminum (Al) layer is to create zero impedance to explain transmission line theory (TLT) and block all incoming EM waves. An absorption system with significant electrical and/or magnetic losses is required to capture the moving waves, and the metal layer at the bottom stops the wave propagation. Through the use of EM waves impinging on the upper plane, absorption parameters were obtained.

In the simulation of micrometer-scale THz MTM absorbers using Computer Simulation Technology (CST) Studio, achieving precision in results is contingent upon meticulous choices regarding conditioning boundaries and wave sources. Employing absorbing boundary layers, particularly perfectly matched layers (PMLs), is essential to prevent undesired reflections and confine energy within the simulation domain, a critical consideration for THz simulations. Ensuring accurate simulation conditions involves employing a domain size significantly larger than the MTM structure to minimize near-field interactions with the boundary layers and ensure precise absorption calculations. Meshing strategies require a fine mesh around the MTM structure, particularly near sharp features, for an accurate representation of intricate EM field distributions at the micrometer scale. Equally critical is the selection of wave sources, with plane wave sources necessitating careful alignment of polarization for uniform illumination in THz simulations, while port sources can be employed for specific cases. Additional considerations encompass exploiting symmetry planes, defining accurate material properties, and utilizing post-processing techniques to analyze absorption spectra and electric field distributions for performance evaluation and design optimization. By judiciously addressing these factors within CST Studio, effective simulations of micrometer-scale THz MTM absorbers can be conducted, yielding valuable insights into absorption properties and potential applications in biosensing. In the design of MTMs as PAs for applications in the micrometer-sized THz range using CST Studio, precision relies on thoughtful consideration of conditioning boundaries and wave sources. Defining conditioning boundary conditions accurately is crucial to capturing the MTM's behavior within the simulation environment, involving the specification of geometric dimensions, material parameters, and the arrangement of subwavelength structures to ensure a faithful representation of the MTM's properties. For THz PAs, the choice of wave source is critical, requiring the use of a broadband and directional THz source to

adequately characterize the MTM's absorption behavior across the desired frequency range. The parameters of the wave source, such as frequency and polarization, must align with the intended application and the resonant features of the MTM. By carefully defining these conditioning boundaries and selecting an appropriate wave source within CST Studio, designers can conduct rigorous simulations to optimize the MTM's performance as a PA in the micrometer-sized THz regime. This facilitates the advancement of tailored designs for biosensing and related applications. Boundary conditions also extend to the interface with the surrounding medium, emphasizing precise control for selective biosensing applications.

The MTMs we designed for THz biosensing, operating at micrometer-scale wavelengths, require meticulous consideration in their design. These MTMs utilize subwavelength structures, often resonators, that are precisely configured to exploit resonant absorption mechanisms within the targeted THz frequency band. Incorporating materials with specific dielectric and metallic properties, these structures induce resonances aligned with the desired THz wavelengths. Tunable parameters, such as geometric dimensions and material properties, are strategically adjusted for optimal absorption efficiency and adaptability to biosensing requirements. Surface functionalization with biomolecular receptors ensures selectivity for analytes, and the micrometer-scale dimensions allow interactions with biomolecules at a biological entity scale. This orchestrated approach to material selection, structural design, and functionalization renders these MTMs suitable for high-resolution, label-free biosensing in diverse biomedical and environmental applications. In particular, MTM-PAs for THz biosensing leverage micrometer-scale, resonant metallic, or dielectric microstructures to achieve ultrahigh absorption at targeted frequencies. These designs create spectral fingerprints and unique absorption profiles corresponding to the vibrational signatures of biomolecules, enabling highly specific and label-free THz biosensing on a miniaturized platform. The label-free approach relies on the exquisite sensitivity of engineered resonant microarchitectures to RI changes induced by biomolecules interacting with the sensor surface, eliminating the need for traditional labeling strategies. This method allows real-time, dynamic monitoring of biomolecular interactions with high precision, offering advanced diagnostic and analytical applications. The spectral fingerprints in THz MTM biosensing refer to unique features within the absorption spectra induced by the interaction with biological analytes. Designed as PAs, MTM structures exhibit distinctive resonant behavior in the THz range, and when functionalized with biomolecular receptors, they selectively interact with target analytes, leading to characteristic shifts or alterations in the absorption spectra. These changes, characterized by specific peaks, dips, or intensity variations, constitute the spectral fingerprints associated with binding events or molecular interactions on the MTM surface. The precise engineering of MTM structures allows for customization of these spectral features, offering a platform for highly sensitive and specific, label-free biosensing in medical diagnostics and biomolecular research.

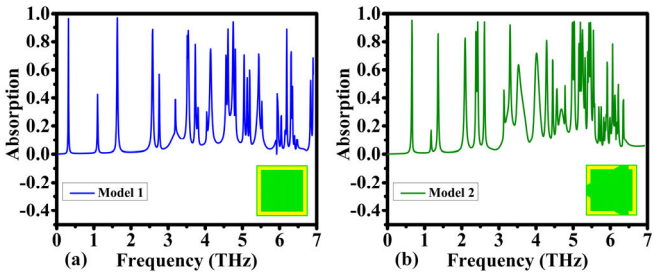

Fig. 2. Absorption characteristics of different designs (a) Model 1 and (b) Model 2.

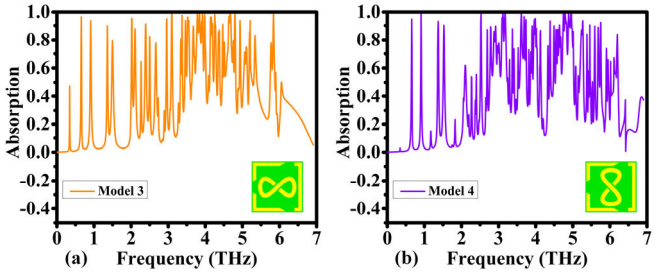

Fig. 3. Absorption characteristics of different designs (a) Model 3 and (b) Model 4.

IV. Results and Discussion

This section will present a thorough investigation, with results applicable to the most sensitive sensors. Using CST Studio, the sensor was designed and simulated. The expression ensures absorption and the ground plane prevents transmission through the model

$$A = 1 - R - T = 1 - |S_{11}|^2 - |S_{21}|^2 . \tag{1}$$

The S parameters for transmission and reflection are denoted as S_{21} and S_{11}, respectively. Therefore, the reflectivity R must be kept as low as possible to achieve maximum absorption.

Six different models were studied in this article. The models move from simple designs to very complex designs. The main objective of presenting these models is to propose a sensor with very high sensitivity for biosensing purposes. Additionally, these six models offer more capabilities for applications ranging from simple to advanced. Designing a sensor to act as a biosensor is not easy and requires a very high level of sensitivity that the sensor can provide. The first model, shown in Fig. 2(a), has a simple design but is highly sensitive. Then, in the second model, a discontinuous square was proposed. The main goal of this design is to prepare a model that can be combined with a relatively advanced infinity design. In the second model, a high-sensitivity region is observed in the frequency range of 5 to 6 THz, as explained in Fig. 2(b). In addition, a relatively complex design is presented in the third and fourth models, and the results of both models show exceptional sensitivity. However, very low sensitivity is observed in both models in the frequency range of 6 to 7 THz, as shown in Fig. 3. Incorporating the infinity design in the third and fourth models, a fifth model has been designed. As explained in Fig. 4(a), it has good sensitivity, but to get a sensor that can distinguish between normal and leukemic blood, we need a very sensitive sensor, so the combination

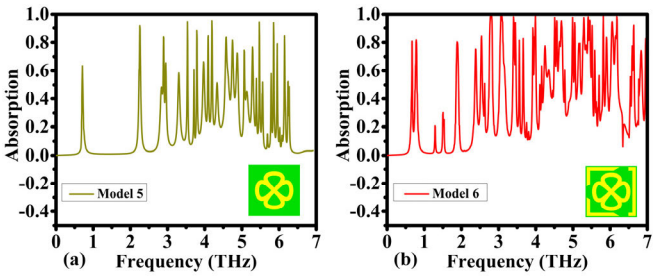

Fig. 4. Absorption characteristics of different designs (a) Model 5 and (b) Model 6 (proposed design).

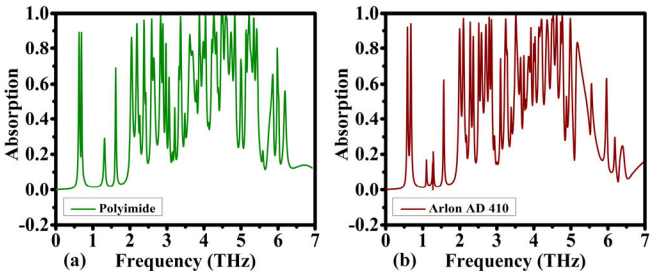

Fig. 5. Absorption spectra for the proposed design under different substrates (a) polyimide and (b) Arlon AD 410.

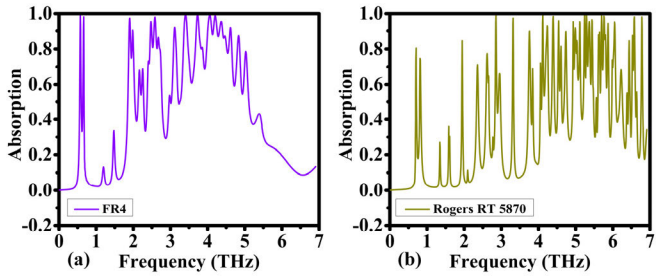

Fig. 6. Absorption spectra for the proposed design under different substrates (a) FR4 and (b) Rogers RT 5870.

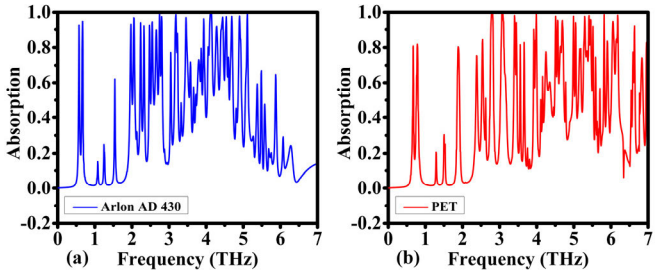

Fig. 7. Absorption spectra for the proposed design under different substrates (a) Arlon AD 410 and (b) PET.

of the fifth and second models has been proposed. The main goal of this combination is to obtain a sensor whose sensitivity remains almost unchanged during the experiment, as shown in Fig. 4(b). The proposed sensor has 29 resonance bands identified as PAs. where each resonance exceeds 80% absorption. It is interesting to note that in this ratio, ten resonance bands can absorb in excess of 97%.

The absorption peaks have been intentionally optimized within the context of our study. However, achieving multiband absorption in narrow frequency ranges presents inherent challenges, particularly in the THz domain. The observed intensity of the peaks is a deliberate feature intended to enhance sensitivity, as discussed in our article. This heightened sensitivity is of paramount importance, particularly in practical applications, where accurate discrimination between healthy and leukemic blood samples is essential. The intensified peaks afford increased opportunities for interaction with blood biomolecules, thereby facilitating a more definitive distinction between the two sample types.

Another study focuses on sensor substrates. Polyimide and Arlon AD 410 were used, as explained in Fig. 5. Both materials showed good sensitivity. However, both materials lose sensitivity at high frequencies, especially in the 5.5 to 7 THz range, as shown in Fig. 5. FR4 was subsequently used, but it is interesting to note that this material has relatively low sensitivity, especially for biosensing purposes. Its sensitivity is relatively low. Furthermore, the FR4 material suffers from a lack of sensitivity at high frequencies, especially above 5 THz, as shown in Fig. 6(a). Subsequently, Rogers RT5870 material was investigated and found to have very good sensitivity and resilience in maintaining high sensitivity at high frequencies, as explained in Fig. 6(b). Arlon AD 430 is also used. After investigation, it was found to have good sensitivity but does not work at high frequencies, especially above the 5 THz band, as shown in Fig. 7(a). Then, PET material was researched and found to have very good sensitivity and preserve its sensitivity even at high frequencies. Especially in the THz frequency range, the PMAs shown in Fig. 7(b) appear to be a very interesting candidate for sensing applications. Designed to create strong resonances in this frequency range, the absorber exhibits increased sensitivity to specific frequencies of EM radiation, opening up the possibility of creating tuned sensors suitable for various cancer detection signatures in the THz range. The unique structure of the absorber consists of an aluminum layer that serves as the metallic reflector and a PET substrate that serves as the dielectric layer. There is a significant increase in the absorption of EM waves at the resonant frequency when the absorber is exposed to the EM wave, as it traps the wave and causes repeated reflections between the PET and aluminum layers. This PMA has potential applications in leukemia detection, among other sensing applications. All things considered, the absorber represents cutting-edge technology with exceptional sensitivity, specificity, and adaptability, making it the top choice for many THz sensing applications.

When comparing Rogers RT5870 with PET as a base material to create an ideal absorber MTM in the THz range, significant advantages and disadvantages arise. Notably, the RT5870 suffers from limitations such as limited data availability for its features at higher THz frequencies, making proper design and optimization difficult. Additionally, this material exhibits small anisotropic behavior, requiring careful consideration of the direction of EM wave propagation when designing the MTM. Additionally, the cost of RT5870 is much higher than PET, raising concerns about commercial feasibility and large-scale production. Despite these issues, RT5870 has advantages over PET, including a lower dielectric constant, a lower loss tangent, higher thermal conductivity, a wider

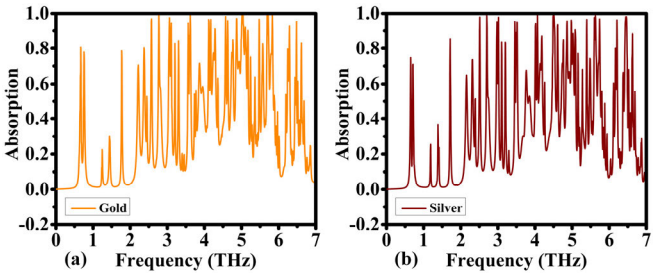

Fig. 8. Absorption spectra for the proposed design under various resonator materials (a) gold and (b) silver.

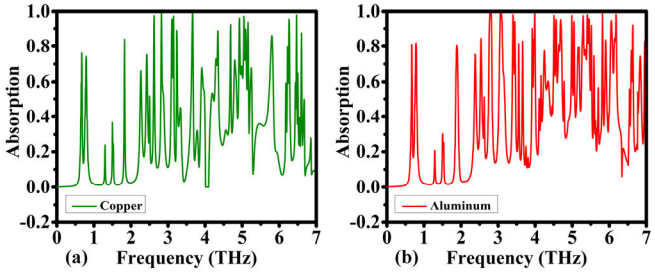

Fig. 9. Absorption spectra for the proposed design under various resonator materials (a) copper and (b) aluminum.

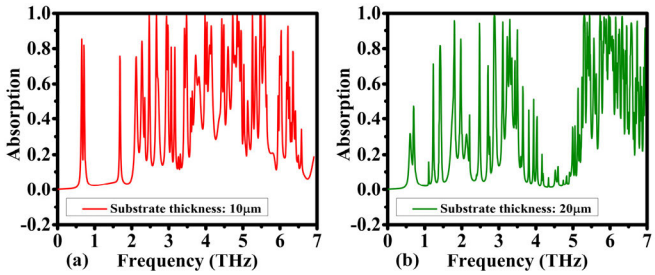

Fig. 10. Effect of substrate thickness on absorption (a) substrate thickness 10 μm and (b) substrate thickness 20 μm.

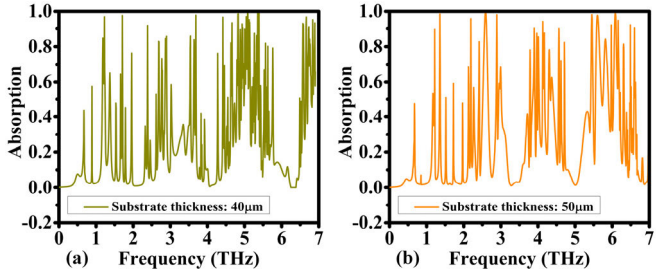

Fig. 11. Effect of substrate thickness on absorption (a) substrate thickness 40 μm and (b) substrate thickness 50 μm.

adjustable thickness range, and better stability. These benefits, however, have to be balanced against the difficulties of choosing a substrate material for particular THz applications. PET has its own set of trade-offs, including a greater dielectric constant, a larger loss tangent, poorer thermal conductivity, a narrower thickness tuning range, and worse dimensional stability, while being more affordable, readily produced, and widely accessible. The decision between RT5870 and PET ultimately comes down to the particular needs of the application, accounting for things like budgetary restrictions, simplicity of production, and the material qualities that are ideal for THz performance.

Next, the resonators' materials—aluminum, copper, silver, and gold—were examined. Fig. 8 illustrates the good sensitivity of gold and silver. According to research, copper has less sensitivity than other conducting materials [see Fig. 9(a)]. The aluminum material was then discovered to have good sensitivity, as shown in Fig. 9(b). The key reasons aluminum was chosen for the proposed sensor are that it is less costly and easier to produce than gold and silver.

Subsequently, it was investigated on the chosen substrate thickness, which is PET, and ranges from 10 to 50 μm. This research is crucial for manufacturing, particularly because of how sensitive the sensor is to variations in PET thickness. The 10 μm measurements demonstrate excellent sensitivity. However, in the 4 to 5 THz frequency region, 20 μm thickness exhibits limited sensitivity. Furthermore, as Fig. 10 explains, it has extremely great sensitivity at high frequencies above 5 THz. Fig. 11 illustrates the extremely good sensitivity of the thicknesses of 40 and 50 μm.

Polarization can cause poor SNR in sensing and imaging applications, thereby distorting results. The symmetry of the proposed structure makes the sensor polarization independent [68], [69]. The complex interaction between polarization angle and incidence angle affects the SNR in THz imaging. The incidence angle represents the angle at which the radiation hits the sensor surface, while the polarization angle describes the direction of the electric field vector of the incident THz radiation. These angles are important for optimizing SNR due to their influence on the interaction of THz waves with the PMA. Some MTM designs are sensitive to different polarization angles, causing changes in the absorbed signal and thus the SNR. Therefore, controlling the polarization of the incident wave is very important to optimize SNR. Similarly, the incidence angle of THz radiation can influence absorption efficiency and SNR, with some MTM designs exhibiting an angle dependence. In practical situations where the incidence angle is variable, careful control of the polarization and incidence angle is necessary to obtain a suitable SNR. For more accurate and reliable THz imaging applications, careful consideration of angles is essential. Precision MTM design determines the complex interaction between polarization angle, incidence angle, and SNR in a THz-perfect MTM absorption sensor. The absorption peak is affected by the polarization angle; for the resonant polarization, the SNR is maximum, but for the other polarizations, the SNR is lower. Due to the change in wave phase difference and path length, the incidence angle leads to angular dependence, affecting the absorption efficiency. Design choices can result in a wide range of angular responses or sensitivities at certain angles. Absorption and SNR are reduced due to loss of coupling at large incidence angles. Generating specific omnidirectional or angular responses based on the shape and characteristics of the MTM is the goal of optimization techniques. For maximum sensitivity, the complex combined effect of polarization and incidence angle on SNR requires careful adjustment of

parameters. Improving the SNR and capabilities of many THz imaging and sensing applications is the goal of ongoing research and development. This is clearly seen in Fig. 12, where there is no barrier because the absorption properties hardly change as the polarization angle changes. Incident angles from 0° to 90° were used in the proposed model. The two extreme absorption regions do not change in different directions, as shown in Fig. 12(a). Additionally, polarization angles ranging from 0° to 90° were used. From Fig. 12(b), both extreme absorption regions do not change over an angular range. This proves that the proposed model operates stably over a wide range of polarization and incidence angles. Further investigation was also performed in the frequency range from 1.7 to 3.6 THz, where nine intense absorption regions could be observed. The results show that no change is observed between the incident angle and the polarization angle as explained in Fig. 13. Subsequently, the frequency range from 3.6 to 5.2 THz was investigated. Ten strong absorption regions were observed in this range. The results demonstrate that there is no obvious difference between the polarization angle and the incidence angle as explained in Fig. 14. Next, the frequency range from 5.2 to 7 THz was investigated. In this range, seven strong absorption regions are observed. The results show that no change is observed between the incident angle and the polarization angle as explained in Fig. 15. The THz imaging process using MTM perfectly absorbing biosensors is significantly affected by the combination of transverse electric (TE) and transverse magnetic (TM) polarization, as well as another different angle of incidence. The anisotropic properties of the MTM lead to distinct resonant frequencies for the TE and TM modes in the THz range, allowing selective enhancement or suppression of specific imaging features depending on the resolution and selected pole. Additionally, the unique electric and magnetic field distributions of the TE and TM modes in the MTM and surrounding tissues lead to diverse near-field interactions and potentially variable sensitivity to biomolecules. The effectiveness of resonant coupling between the THz wave and the MTM structure varies depending on the angle of incidence, affecting the overall intensity and spatial distribution of the enhanced field in the tissue, and thereby affecting the compatibility, contrast, and resolution of the image. The angle of incidence, especially for specific MTM designs, can impact the surface plasmon resonance, thereby enhancing light-matter interactions and further changing the THz imaging properties. The combined effects of TE/TM polarization and different incidence angles create a complex interaction landscape, highlighting the importance of optimizing both parameters to tune the THz imaging response. Understanding these effects is critical for refining the design and performance of MTM biosensors for THz imaging. By meticulously controlling these parameters, researchers can tailor the response of the image, improving sensitivity and specificity in detecting specific molecules or features in tissue. This promises advances in early cancer detection and other diagnostic applications, as TE/TM polarization and different incident angles provide additional dimensions for control and optimization and interaction between THz waves and biological sensors. To verify the

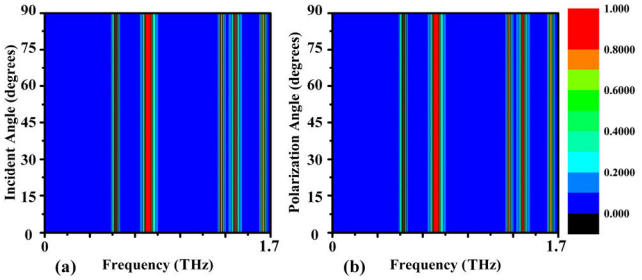

Fig. 12. Effect of angle variation on absorption rate (0–1.7 THz) (a) incidence angle and (b) polarization angle.

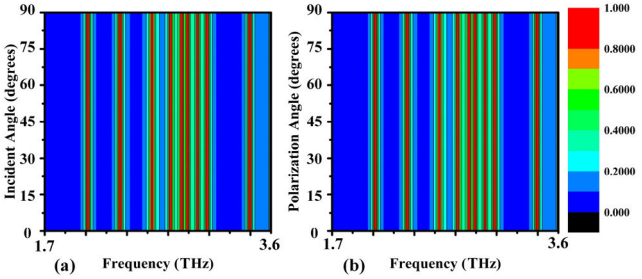

Fig. 13. Effect of angle variation on absorption rate (1.7–3.6 THz) (a) incidence angle and (b) polarization angle.

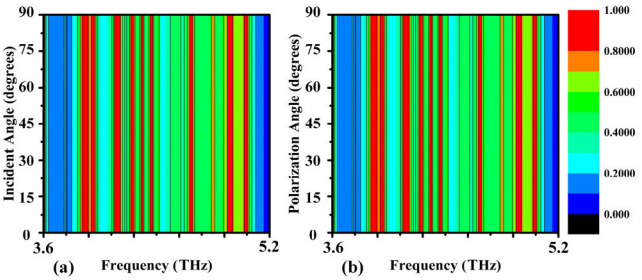

Fig. 14. Effect of angle variation on absorption rate (3.6–5.2 THz) (a) incidence angle and (b) polarization angle.

sensitivity of the biosensor during MWI for early detection of leukemia, a detailed study was performed for TE and TM at different angles from 0° to 90° as explained in Fig. 16. The results for TE ensure that the proposed biosensor is capable of reconstructing very high-resolution images as it does not suffer from multiband loss, as explained shown in Fig. 16(a). However, as you can see in the figure, TE does not change for different incidence angles except for 75°. However, these peaks were not chosen as PAs because their absorption is less than 80% (the green line is between 6 and 7 THz), so the difference can be neglected. Subsequent detailed studies of the TM showed that it maintained biosensor performance from all angles. The results provide high confidence in the biosensor's ability to detect leukemia at an early stage with very high-quality deterministic images, as shown in Fig. 16(b).

After testing the electric field, Fig. 17(a) demonstrates that the high electric field density of the recommended sensor contributes to its outstanding performance in biomedical sensing applications. These field distributions help understand design performance and provide insight into the resonance process. Deciphering E-field distributions in CST Studio

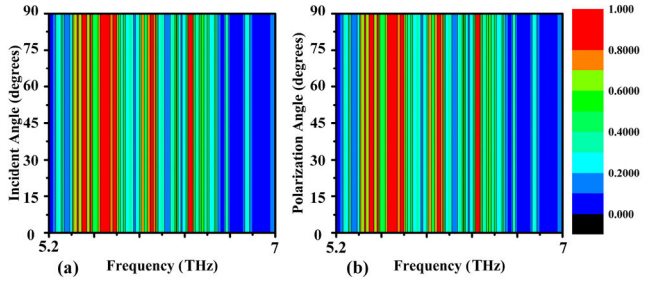

Fig. 15. Effect of angle variation on absorption rate (5.2–7 THz) (a) incidence angle and (b) polarization angle.

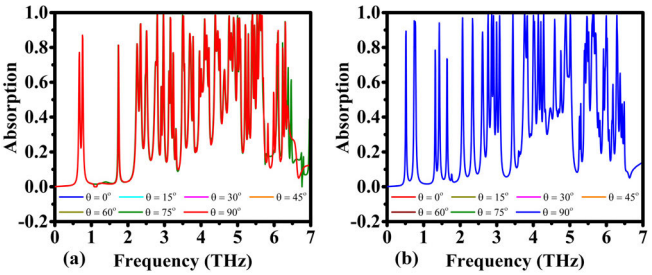

Fig. 16. Effect of angle variation on absorption rate (0–7 THz) (a) TE and (b) TM.

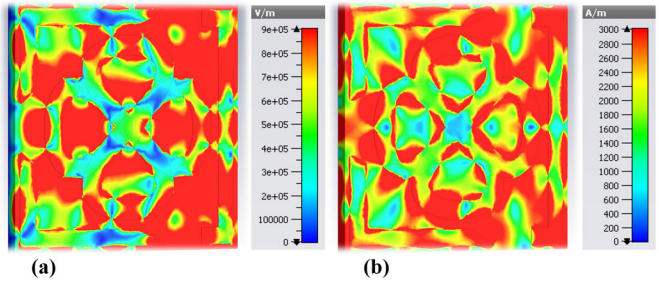

Fig. 17. Field distributions of the MTM structure (a) *E*-field and (b) *H*-field.

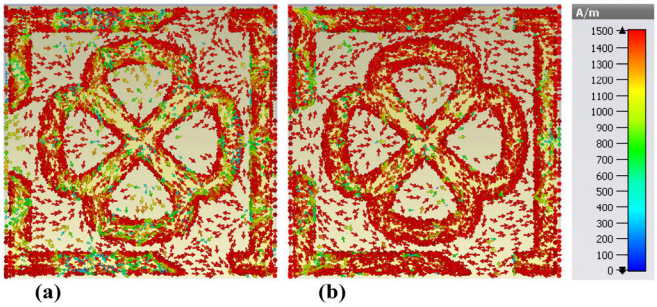

Fig. 18. Surface current distribution of the recommended MTM (a) imaginary part and (b) real part.

during the design of MTM PAs (MTMPAs) involves a dual strategy. Analyzing the z-component, Ez, reveals insights into localized light-matter interaction. Elevated Ez values identify regions of intense field confinement, often around sharp features or metallic resonators, indicating crucial locations for efficient energy conversion into heat—a key factor in achieving near-perfect absorption. Scrutinizing Ez variations near specific features provides an understanding of local resonance behavior, aiding in field channeling optimization. Additionally, examining the magnitude of the E-field, $|E|$, offers a holistic view by revealing hot spots—areas of concentrated energy critical for overall absorption efficiency. Analyzing the $|E|$ profile across the entire structure unveils potential leakage or scattering losses, guiding optimization efforts to minimize energy escape and achieve near-perfect absorption. The synergistic analysis of Ez for localized interaction and $|E|$ for global field distribution empowers a comprehensive understanding of MTM behavior, facilitating robust design optimization and peak THz absorption performance. This scientific approach, coupled with CST Studio's simulation capabilities, serves as a key driver in the realm of MTMPAs design. Analysis of the electric field strength at different frequencies clearly shows how specific components contribute to signal resonance. The multiband sensor effectively absorbs EM radiation at different frequencies in the THz range, as demonstrated by the electric field distribution. The electric field strength in the MTM structure, influenced by features such as metallic resonators and dielectric substrates, enhances absorption at specific frequencies. Multiple peaks in the electric field intensity correspond to the sensor's multiband functionality, allowing it to detect and differentiate between THz wavelengths for versatile sensing applications. This visualization provides valuable insight into the functionality of the multiband perfect MTM absorption sensor. A very dense circular region of magnetic field is shown in Fig. 17(b), indicating the high sensitivity of the proposed sensor. This strong magnetic field prevents any change in polarization angle, which demonstrates the outstanding performance of the proposed sensor in biological imaging and biosensing. This high magnetic density indicates a high sensitivity to the absorption of EM waves.

The surface current distribution of the upper layers of the proposed design was investigated to better understand the physical absorption process of the proposed MTM absorbers. The proposed sensor will have both real and imaginary components as it is made from MTMs. The antiparallel current flows in a circular pattern, indicating a strong magnetic response. Fig. 18(a), which shows the parallel and antiparallel surface current patterns for the imaginary component, also presents the magnetic dipole resonance mode. Sometimes the surface current on metal layers can go in the opposite direction. Antiparallel circular currents indicate the presence of a strong magnetic response. This relates the incident H-field to the magnetic flux. A strong response to a magnetic field is demonstrated by an antiparallel circular current. Whether the currents are parallel or antiparallel, their distribution determines the distribution of the electric and magnetic fields, as explained in Fig. 18(a). The external magnetic field (H-field) will oppose the internal magnetic field created by the parallel flow, and vice versa.

The surface current density of the real part of the multiband THz sensor was investigated, showing a symbiotic relationship with the electric field distribution, as shown in Fig. 18(b). Bright regions on the MTM surface correspond to increased current concentrations, reflecting strong electric field regions

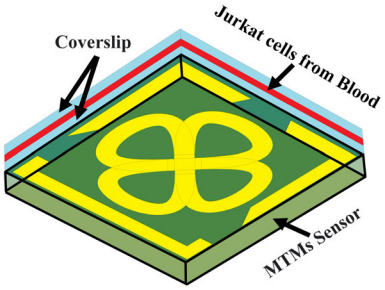

Fig. 19. Absorption coefficient studies in healthy and cancerous blood.

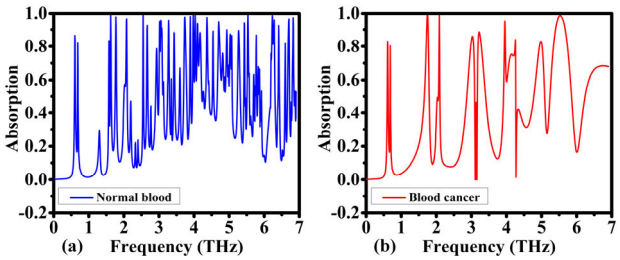

Fig. 20. Absorption coefficients in the frequency range (0–7 THz) (a) normal blood and (b) blood cancer.

and their role in effectively absorbing THz at specific frequencies. The circular or ring-shaped current patterns surrounding the metallic resonator reveal the MTM's inherent resonant modes, which give rise to absorption at distinct THz wavelengths. The surface current density distribution supports the multiband functionality of the sensor through multiple circulating currents at various locations, revealing intentional resonance at multiple frequencies for effective absorption in many different frequency bands in the THz range.

V. Blood Cancer Diagnosis

The leukemia diagnostic biosensor is an attractive sensor that uses advanced technology to detect and diagnose leukemia in its early stages. Using MWI, the sensor can appropriately model and measure signal transmission and absorption, thereby improving efficiency in identifying cancer cells. This unique approach addresses current barriers to quickly and effectively diagnosing leukemia, perhaps offering a solution to improve early detection and diagnosis. Fig. 19 shows how the proposed sensor can detect leukemia. We use two coverslips to provide error-free results. A Jurkat cell is prepared from a blood sample placed between these two coverslips, as shown in Fig. 19. Diagnosis is made using a RI of 1.376 for healthy blood and 1.39 for leukemia, respectively [70], [71], [72], [73], [74]. As shown in Fig. 20, the data were analyzed for normal blood and newly malignant blood. Fig. 20(a) shows the results of normal blood. It is also shown in Fig. 20(b) for blood with early-stage malignancy. The results show very significant differences, which confirms the outstanding performance of the proposed sensor and its reliability among specialized hematologists. The figure of merit (FOM) and Q-factor are crucial metrics for evaluating the performance of multiband PA MTMs as sensors. The FOM calculates the efficiency of a sensor by dividing a performance parameter like sensitivity by another factor like bandwidth or noise level. The Q-factor, a dimensionless parameter, measures the quality of resonance in the system. Higher values for both FOM and Q-factor indicate superior performance, making them essential for evaluating the effectiveness of multiband PA MTMs in sensor applications. The sensitivity of MTM-PAs is determined by their ability to respond to changes in the RI of the surrounding medium. This sensitivity is measured by the change in the resonant frequency or absorption peak of the absorber. The higher sensitivity indicates the ability to detect and differentiate small changes in RI, making it suitable for applications such as early-stage cancer detection. Sensitivity is important to obtain accurate measurements in situations with large variations in RI.

The FOM, Q-factor, and sensitivity (S) of a sensor are three of its most essential characteristics for determining its performance. The selectivity of a sensor is indicated by its full output measurement FOM, which is equal to the normalization of the sensitivity to the resonant dip's full width at half maximum (FWHM)

$$\text{FOM} = \frac{S}{\text{FWHM}}. \tag{2}$$

The Q_{factor}, which has the formula, is used to quantify the resonance sharpness

$$Q_{\text{factor}} = \frac{\lambda}{\text{FWHM}} \tag{3}$$

resonance wavelength, expressed as λ. MTM-based THz biosensor comprehensively improves THz detection sensitivity. In our study, sensitivity is assessed by the biosensor's capability to detect changes in RI per unit shift in THz frequency. The sensitivity (S) metric reflects the rate of THz frequency change per RI units (RIU), indicating the biosensor's ability to detect minute fluctuations in sample RI. While traditional sensor evaluations focus on specific peaks, our multiband biosensor operates across a wide frequency range, allowing for a comprehensive assessment of sensitivity across all bands. This approach highlights the biosensor's efficacy in early-stage leukemia diagnosis by detecting subtle blood RI variations, enhancing its clinical utility. The scientific literature often uses two meanings of sensitivity. The first is frequency sensitivity

$$S = \frac{\Delta f}{\Delta n} \tag{4}$$

where Δn is the change in RI, usually expressed as a function of RIU, and Δf is the frequency shift of the resonance peak. An alternative approach is to compute $S = \Delta I/\Delta n$, the intensity frequency, where ΔI is the resonant intensity variation [75], [76].

A penicillin detection biosensor based on MTMs was shown, with a FOM of 0.1216 RIU^{-1}, a Q-factor of 5.58, and sensitivity (S) of 0.02432 THz/RIU. A different biosensor with a Q-factor of 2.43, a FOM of 2.75 RIU^{-1}, and 1.21 THz/RIU was created for the detection of breast cancer. Additionally, a different biosensor with a sensitivity (S) of 1.06 THz/RIU and an FOM of 0.166 RIU^{-1}—which is not specified as a Q-factor—was created for the purpose of detecting the

TABLE II
COMPARISONS OF BIO-SENSING PERFORMANCE OF VARIOUS SENSOR APPLICATIONS BASED ON THZ MTM

References	Bio-application	Q	S (THz/RIU)	FOM (RIU−1)	Year Published
[30]	detection of Penicillia	5.58	0.02432	0.1216	2014
[36]	detection of Virus	-	0.0242, 0.02438	-	2017
[77]	sensor	6.6	0.285	1.88	2020
[78]	Biosensor, Collagen	-	0. 960	-	2020
[79]	Polystyrene particle	-	0. 2833	-	2021
[80]	cancer detection	-	1.6498	11.33	2021
[81]	Cancer Diagnosi, Biosensor	2.43	1.21	2.75	2022
[82]	sensor	8.21, 6.05	0. 203	1.81, 1.57	2022
[83]	detection of avian influenza virus	-	1.06	0.166	2022
[84]	SARS-CoV-2 virus	-	0.49	0.377	2022
This work	Blood cancer Diagnostics	41.1	18626373	172466416	-

avian influenza virus. We propose a multiband biosensor. The biosensor provided in this article is presented with a Q-factor of 41.1, a FOM of 172 466 416 RIU^{-1}, and a sensitivity (S) of 18 626 373 THz/RIU, presented for the diagnosis of leukemia, as explained in Table II.

Our findings may open new possibilities for relevant applications in leukemia research by comparing previously created biosensors, especially for biological applications, based on the assessment of their physical quality for biosensing. This large difference in frequency helps diagnose leukemia using THz imaging. By examining the THz frequency spectrum in a patient's blood, healthcare professionals can accurately detect and diagnose leukemia, allowing for early intervention and treatment.

MTM-based THz imaging for biosensing involves the use of artificial materials (MTMs) in the THz frequency range to examine and detect biological materials. Combining the specialized properties of MTMs with the specific properties of THz radiation improves sensitivity and specificity in biosensing applications. Using the unique properties of MTMs, a revolutionary THz imaging technique for biosensing enhances the sensitivity, selectivity, and real-time imaging capabilities of THz technology to identify and test biological materials. Leukemia can be identified and visualized using THz imaging, helping with early identification and treatment. This noninvasive technique could radically change the field of hematology by providing a reliable and effective method for identifying blood cancers. Because of its special qualities, such as its ability to penetrate the bloodstream and provide molecular details, THz radiation can be used to identify abnormalities associated with leukemia. The THz imaging presented in this article is based on the dielectric properties of healthy blood and newly discovered cancers. This leads to a difference in RI. The RI of cancerous blood is higher than that of healthy blood. As a result, the electric and magnetic fields have different strengths. Cancer cells are more sensitive to electric and magnetic fields than normal blood cells. This difference shows a strong ability to distinguish leukemia from healthy blood. This is important because the variation in size and shape of the Jurkat cells produced from blood does not affect the results.

Leukemia can be detected more easily using the unique properties of THz waves, especially when using MTMPAs as sensors. Indeed, waves can penetrate biological tissues and interact with molecular vibrations and the rotational modes of blood. Certain THz frequencies are resonated by the MTMPA's engineered structure, which includes a metal reflector plate such as aluminum and a dielectric layer such as PET. MTMPAs undergo resonance when exposed to THz radiation, causing a significant increase in absorption at its resonant frequency. In terms of leukemia diagnosis, the sensitivity of MTMPAs helps identify small changes in the THz absorption spectrum associated with WBCs. Because of its sensitivity, MTMPAs can distinguish leukemia cells from healthy blood cells by identifying distinct THz signals that correlate with genetic or structural features specific to the disease. Researchers can detect the existence of leukemia cells by looking at the change in the resonance frequency or absorption peak of an absorber. This method provides a noninvasive method for the early detection and monitoring of leukemia. This article highlights how THz technology, combined with complex sensor designs such as MTMPAs, can significantly improve medical diagnostics by improving sensitivity and specificity.

As shown in Table III, the proposed biosensor used for THz imaging is based on MWI, which is contrary to the research reported in the literature. The RI changes we observe in the frequency domain data provide us with spatial insight into the target. Understanding these differences is necessary to reconstruct the image, which shows the internal structure of the target. In THz imaging in the frequency domain, the phase changes of THz waves as they pass through or interact with materials provide important information about the material's properties. The change in the RI of the target causes a phase shift of the THz waves in different regions of the target during imaging. By monitoring these phase transitions at different times, we can estimate the internal structure of the target in spatial terms. The spatial distribution of the RI variations is then used to reconstruct the image. To create an image illustrating these fluctuations, the spatial distribution of RI variations is used to reconstruct the image.

The results were confirmed using MWI techniques based on the basic principles of image reconstruction in the THz spectrum described above. To test the sample using the proposed biosensor, a blood sample was placed on a coverslip as shown in Fig. 21. The results are presented as images of different properties of the proposed sensor. Fig. 22 shows the electric field data obtained from MWI. Normal blood detects a weak electric field, as shown in Fig. 22(a). However, as shown in Fig. 22(b), the bright red spot indicates a very high electric field density, implying that the sample is leukemia. This implies that, by using electric field measurements as a basis, MWI can effectively differentiate healthy blood tissue from

TABLE III
COMPARISON BETWEEN THE THZ BAND STUDY ON PERFECT MTMS AND THE RECOMMENDED BIOSENSOR

References	Techniques used	Frequency operating THz	Material substrate	Absorptivity	Application
[85]	Ion gel/Graphene/Teflon/Gold	0.7-5	Teflon	>0.96	polarization-sensitive
[86]	graphene/Topas/Au	0.5−4.5	Topas spacer	0.99, 0.98, 0.99	Ultra-Broadband Absorber
[87]	bulk Dirac semimetal/photonic crystal/Au	1−3	photonic crystal plate	0.97, 0.98, 0.99	Narrowband perfect absorber
[88]	Au/dielectric layer/Au	1−3	dielectric layer	0.99, 0.99	Sensor
[89]	PET/FSS/UV glue/ Graphene	0-3	PET	0.99, 0.80, 0.95	Multifunctional Tunable Terahertz
[90]	Au/SiO2/ Graphene	7-9.5	SiO2	0.98	Multi-Frequency Broadband and Ultra-Broadband
[91]	Gold/silicon dioxide/ Gold	1.5-1.7	silicon dioxide	0.972, 0.991	biosensor for detecting coronaviruses
[92]	Glass/InSb/MgF2/InSb	0-0.37	Glass	0.998	Colon Cancer Detection
[81]	SiO2/Graphene	0.5-2.5	SiO2	-	Breast cancer detection
[93]	Au/dielectric Teflon/Au	1−2.2	dielectric Teflon	0.99	Sensor
[94]	graphene/Au/SiO2/Au	2−6	SiO2	0.99	Refractive index sensor
This work	Al/PET/Al	0−7	PET	Ten peaks: >0.97 Seven peaks: >0.98 Three peaks: >0.996	Biosensor, Blood Cancer Diagnostics and Microwave Imaging

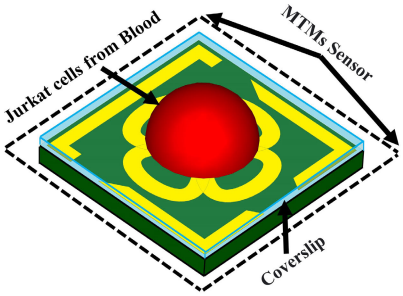

Fig. 21. Blood cancer diagnosis using MWI technique.

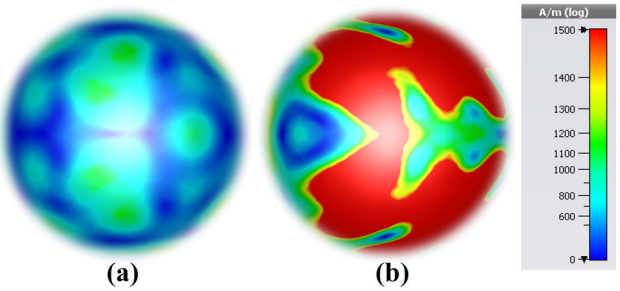

Fig. 23. *H*-field MWI-technique results (a) normal blood and (b) blood cancer.

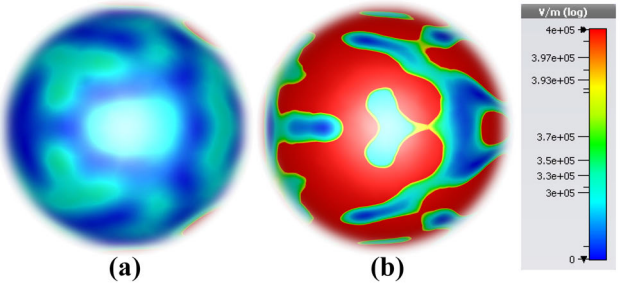

Fig. 22. *E*-field MWI-technique results (a) normal blood and (b) blood cancer.

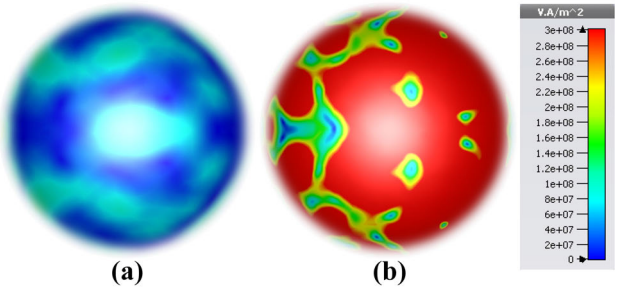

Fig. 24. *P*-field MWI-technique results (a) normal blood and (b) blood cancer.

cancerous tissue. Early identification and effective treatment of leukemia depend on the ability to identify and differentiate malignant tissues. This function allows noninvasive real-time monitoring of tissue abnormalities, which is especially useful in the early detection and diagnosis of leukemia. Additionally, the clinical use of MWI goes beyond diagnosis as it can be used to assess treatment response.

Additional investigations were also conducted to confirm the results. A thorough examination of the magnetic field was performed, as shown in Fig. 23. A region of low-intensity magnetic field was sensed in Fig. 23(a), indicating the existence of healthy blood. On the other hand, as shown in Fig. 23(b), the saturated red region indicates a high magnetic field level. This finding suggests leukemia. Further research into the link between magnetic field strength and leukemia has revealed a strong correlation between locations with high magnetic fields and the disease. These results show that magnetic field analysis can be applied to diagnose leukemia. Fig. 24 illustrates another intriguing finding related to power flow. Fig. 24(a) shows a relatively low power, which is a clear indication of healthy blood. However, the presence of a high-power region implies leukemia, as shown in Fig. 24(b). This

discovery shows that biosensors, by providing more accurate and efficient detection techniques, could transform leukemia diagnosis. Biosensors can identify the early stages of leukemia, allowing for early diagnosis and treatment. For leukemia patients to have a better prognosis and survival rate, early detection and treatment are essential. Better patient outcomes may result from early intervention by healthcare professionals using biosensors to identify specific biomarkers associated with leukemia.

VI. Future Perspective

Early-stage diagnosis of adrenal gland cancer (PC-12), cervical cancer (HeLa), colon cancer, breast cancer, and non-melanoma skin cancer using THz EM wave imaging biosensors.

VII. Conclusion

In this article, an advanced and highly sensitive biosensor based on PMAs is introduced, comprising three layers with a ground layer and resonator made of 0.02-μm-thick aluminum and a 10-μm-thick PET material serving as the sensor substrate. The biosensor's design is meticulously analyzed across various models, substrate materials, resonant materials, and substrate thicknesses, demonstrating robust sensitivity to changes and ensuring resilience during the manufacturing process. The biosensor exhibits remarkable sensitivity to different polarization and incidence angles, crucial for THz imaging in hematological applications. Detailed studies on TE with TM at different angles, electric field distribution, magnetic field distribution, and surface current density for both imaginary and real parts further validate its sensitivity performance. Comparative analyses with previously designed sensors highlight the biosensor's exceptional attributes, including a Q-factor of 41.1, a FOM of 172 466 416 RIU^{-1}, and a sensitivity (S) of 18 626 373 THz/RIU. The biosensor's high sensitivity is leveraged for early-stage leukemia detection, showcasing its capacity to differentiate between normal and cancerous blood. Additionally, the use of THz waves for imaging reveals significant distinctions between normal and cancerous blood in MWI, providing hematologists with a valuable alternative for improved early detection, thereby enhancing leukemia cure rates.

References

[1] M. J. Thun, J. O. DeLancey, M. M. Center, A. Jemal, and E. M. Ward, "The global burden of cancer: Priorities for prevention," *Carcinogenesis*, vol. 31, no. 1, pp. 100–110, Jan. 2010.

[2] J. Okikiolu, R. Dillon, and K. Raj, "Acute leukaemia," *Medicine*, vol. 49, no. 5, pp. 274–281, 2021.

[3] J. J. Hutter, "Childhood leukemia," *Pediatrics Rev.*, vol. 31, no. 6, pp. 234–241, 2010.

[4] Y. Zhao, Y. Wang, and S. Ma, "Racial differences in four leukemia subtypes: Comprehensive descriptive epidemiology," *Sci. Rep.*, vol. 8, no. 1, p. 548, Jan. 2018.

[5] M. E. Karar, B. Alotaibi, and M. Alotaibi, "Intelligent medical IoT-enabled automated microscopic image diagnosis of acute blood cancers," *Sensors*, vol. 22, no. 6, p. 2348, Mar. 2022.

[6] F. Bray, J. Ferlay, I. Soerjomataram, R. L. Siegel, L. A. Torre, and A. Jemal, "Global cancer statistics 2018: GLOBOCAN estimates of incidence and mortality worldwide for 36 cancers in 185 countries," *CA Cancer J. Clinicians*, vol. 68, no. 6, pp. 394–424, 2018.

[7] F. Huang, P. Guang, F. Li, X. Liu, W. Zhang, and W. Huang, "AML, ALL, and CML classification and diagnosis based on bone marrow cell morphology combined with convolutional neural network: A STARD compliant diagnosis research," *Medicine*, vol. 99, no. 45, Nov. 2020, Art. no. e23154.

[8] N. Howlader et al., "SEER cancer statistics review, 1975–2013," *Nat. Cancer Inst.*, vol. 19, pp. 1975–2013, 2016.

[9] T. Terwilliger and M. Abdul-Hay, "Acute lymphoblastic leukemia: A comprehensive review and 2017 update," *Blood Cancer J.*, vol. 7, no. 6, p. e577, Jun. 2017.

[10] S. Paul, H. Kantarjian, and E. J. Jabbour, "Adult acute lymphoblastic leukemia," *Mayo Clinic Proc.*, vol. 91, no. 11, pp. 1645–1666, 2016.

[11] E. Jabbour, S. O'Brien, M. Konopleva, and H. Kantarjian, "New insights into the pathophysiology and therapy of adult acute lymphoblastic leukemia," *Cancer*, vol. 121, no. 15, pp. 2517–2528, Aug. 2015.

[12] I. Abunadi and E. M. Senan, "Multi-method diagnosis of blood microscopic sample for early detection of acute lymphoblastic leukemia based on deep learning and hybrid techniques," *Sensors*, vol. 22, no. 4, p. 1629, Feb. 2022.

[13] J. B. Baxter and G. W. Guglietta, "Terahertz spectroscopy," *Anal. Chem.*, vol. 83, no. 12, pp. 4342–4368, 2011.

[14] M. Beruete and I. Jáuregui-López, "Terahertz sensing based on metasurfaces," *Adv. Opt. Mater.*, vol. 8, no. 3, Feb. 2020, Art. no. 1900721.

[15] H. Lindley-Hatcher, R. I. Stantchev, X. Chen, A. I. Hernandez-Serrano, J. Hardwicke, and E. Pickwell-MacPherson, "Real time THz imaging—Opportunities and challenges for skin cancer detection," *Appl. Phys. Lett.*, vol. 118, no. 23, pp. 230501-1–230501-6, Jun. 2021, doi: 10.1063/5.0055259.

[16] S. J. Oh et al., "Nanoparticle-enabled terahertz imaging for cancer diagnosis," *Opt. Exp.*, vol. 17, no. 5, p. 3469, 2009.

[17] Z. Vafapour, A. Keshavarz, and H. Ghahraloud, "The potential of terahertz sensing for cancer diagnosis," *Heliyon*, vol. 6, no. 12, Dec. 2020, Art. no. e05623.

[18] W. L. Chan, J. Deibel, and D. M. Mittleman, "Imaging with terahertz radiation," *Rep. Prog. Phys.*, vol. 70, no. 8, p. 1325, 2007.

[19] V. P. Wallace, E. MacPherson, J. A. Zeitler, and C. Reid, "Three-dimensional imaging of optically opaque materials using nonionizing terahertz radiation," *J. Opt. Soc. Amer. A, Opt. Image Sci.*, vol. 25, no. 12, p. 3120, 2008.

[20] Q. Wang, Y. Chen, J. Mao, F. Yang, and N. Wang, "Metasurface-assisted terahertz sensing," *Sensors*, vol. 23, no. 13, p. 5902, Jun. 2023.

[21] Z. Xu, Y. Wang, S. Liu, J. Ma, S. Fang, and H. Wu, "Metamaterials with analogous electromagnetically induced transparency and related sensor designs—A review," *IEEE Sensors J.*, vol. 23, no. 7, pp. 6378–6396, Apr. 2023.

[22] V. G. Veselago, "The electrodynamics of substances with simultaneously negative values of img align=absmiddle Alt=ϵ Eps/Img and μ," *Physics-Uspekhi*, vol. 10, no. 4, pp. 509–514, 1968.

[23] A. F. Almutairi, M. S. Islam, M. Samsuzzaman, M. T. Islam, N. Misran, and M. T. Islam, "A complementary split ring resonator based metamaterial with effective medium ratio for C-band microwave applications," *Results Phys.*, vol. 15, Dec. 2019, Art. no. 102675.

[24] M. Z. Mahmud, M. T. Islam, N. Misran, S. Kibria, and M. Samsuzzaman, "Microwave imaging for breast tumor detection using uniplanar AMC based CPW-fed microstrip antenna," *IEEE Access*, vol. 6, pp. 44763–44775, 2018.

[25] N. Misran, S. H. Yusop, M. T. Islam, and M. Y. Ismail, "Analysis of parameterization substrate thickness and permittivity for concentric split ring square reflectarray element," *Jurnal Kejuruteraan, J. Eng.*, vol. 23, pp. 11–16, Nov. 2012.

[26] A. Rahman, M. T. Islam, M. J. Singh, S. Kibria, and M. Akhtaruzzaman, "Electromagnetic performances analysis of an ultra-wideband and flexible material antenna in microwave breast imaging: To implement a wearable medical bra," *Sci. Rep.*, vol. 6, no. 1, p. 38906, Dec. 2016.

[27] M. Rokunuzzaman, M. Samsuzzaman, and M. T. Islam, "Unidirectional wideband 3-D antenna for human head-imaging application," *IEEE Antennas Wireless Propag. Lett.*, vol. 16, pp. 169–172, 2017.

[28] A. N. Z. Rashed, A. E.-N.-A. Mohammed, W. F. Zaky, I. Amiri, and P. Yupapin, "The switching of optoelectronics to full optical computing operations based on nonlinear metamaterials," *Results Phys.*, vol. 13, Jun. 2019, Art. no. 102152.

[29] I. Al-Naib et al., "Excitation of a high-Q subradiant resonance mode in mirrored single-gap asymmetric split ring resonator terahertz metamaterials," *Appl. Phys. Lett.*, vol. 101, no. 7, Aug. 2012, Art. no. 071108.

[30] S. J. Park et al., "Detection of microorganisms using terahertz metamaterials," *Sci. Rep.*, vol. 4, no. 1, p. 4988, May 2014.

[31] X. Zhang et al., "Polarization-independent plasmon-induced transparency in a fourfold symmetric terahertz metamaterial," *IEEE J. Sel. Topics Quantum Electron.*, vol. 19, no. 1, Jan. 2013, Art. no. 8400707.

[32] F. Hu, L. Zhang, X. Xu, Y. Wang, T. Zou, and W. Zhang, "Study on split-ring-resonator based terahertz sensor and its application to the identification of product oil," *Opt. Quantum Electron.*, vol. 47, no. 8, pp. 2867–2879, Aug. 2015.

[33] H.-M. Li et al., "Electromagnetically induced transparency with large delay-bandwidth product induced by magnetic resonance near field coupling to electric resonance," *Appl. Phys. Lett.*, vol. 106, no. 11, pp. 114101-1–114101-4, Mar. 2015, doi: 10.1063/1.4915313.

[34] L. Xie, W. Gao, J. Shu, Y. Ying, and J. Kono, "Extraordinary sensitivity enhancement by metasurfaces in terahertz detection of antibiotics," *Sci. Rep.*, vol. 5, no. 1, p. 8671, Mar. 2015.

[35] T. Guo and C. Argyropoulos, "Broadband polarizers based on graphene metasurfaces," *Opt. Lett.*, vol. 41, no. 23, p. 5592, 2016.

[36] S. J. Park, S. H. Cha, G. A. Shin, and Y. H. Ahn, "Sensing viruses using terahertz nano-gap metamaterials," *Biomed. Opt. Exp.*, vol. 8, no. 8, pp. 3551–3558, 2017.

[37] Z. Vafapour and M. R. Forouzeshfard, "Disappearance of plasmonically induced reflectance by breaking symmetry in metamaterials," *Plasmonics*, vol. 12, no. 5, pp. 1331–1342, Oct. 2017.

[38] V. Shukla, N. K. Jena, A. Grigoriev, and R. Ahuja, "Prospects of graphene-hBN heterostructure nanogap for DNA sequencing," *ACS Appl. Mater. Interface*, vol. 9, no. 46, pp. 39945–39952, 2017.

[39] T. Ma, Q. Huang, H. He, Y. Zhao, X. Lin, and Y. Lu, "All-dielectric metamaterial analogue of electromagnetically induced transparency and its sensing application in terahertz range," *Opt. Exp.*, vol. 27, no. 12, p. 16624, 2019.

[40] X. Yan et al., "The terahertz electromagnetically induced transparency-like metamaterials for sensitive biosensors in the detection of cancer cells," *Biosensors Bioelectron.*, vol. 126, pp. 485–492, Feb. 2019.

[41] C. Vieu et al., "Electron beam lithography: Resolution limits and applications," *Appl. Surf. Sci.*, vol. 164, nos. 1–4, pp. 111–117, Sep. 2000.

[42] H.-R. Park, S. Namgung, X. Chen, and S.-H. Oh, "High-density metallic nanogap arrays for the sensitive detection of single-walled carbon nanotube thin films," *Faraday Discuss.*, vol. 178, pp. 195–201, 2015.

[43] K. Chen, C. Ruan, and Y. Cao, "SRRs and cross combine asymmetric metamaterials promising for THz sensor," in *Proc. Int. Conf. Microw. Millim. Wave Technol. (ICMMT)*, Sep. 2020, pp. 1–3.

[44] R. Singh, I. A. I. Al-Naib, M. Koch, and W. Zhang, "Sharp Fano resonances in THz metamaterials," *Opt. Exp.*, vol. 19, no. 7, p. 6312, 2011.

[45] K. Chen, C. Ruan, and Y. Cao, "Nano gap metamaterials promising for virus detection," in *Proc. Int. Conf. Microw. Millim. Wave Technol. (ICMMT)*, May 2021, pp. 1–3.

[46] H. Zhang, Y. Cheng, and F. Chen, "Quad-band plasmonic perfect absorber using all-metal nanostructure metasurface for refractive index sensing," *Optik*, vol. 229, Mar. 2021, Art. no. 166300.

[47] J. Zhang et al., "Highly sensitive detection of malignant glioma cells using metamaterial-inspired THz biosensor based on electromagnetically induced transparency," *Biosensors Bioelectron.*, vol. 185, Aug. 2021, Art. no. 113241.

[48] Z. Vafapour, M. Dutta, and M. A. Stroscio, "Sensing, switching and modulating applications of a superconducting THz metamaterial," *IEEE Sensors J.*, vol. 21, no. 13, pp. 15187–15195, Jul. 2021.

[49] A. Hamouleh-Alipour, M. Forouzeshfard, R. Baghbani, and Z. Vafapour, "Blood hemoglobin concentration sensing by optical nano biosensor-based plasmonic metasurface: A feasibility study," *IEEE Trans. Nanotechnol.*, vol. 21, pp. 620–628, 2022.

[50] Z. Vafapour, "Cost-effective bull's eye aperture-style multi-band metamaterial absorber at sub-THz band: Design, numerical analysis, and physical interpretation," *Sensors*, vol. 22, no. 8, p. 2892, Apr. 2022.

[51] B. Karki, A. Uniyal, A. Pal, and V. Srivastava, "Advances in surface plasmon resonance-based biosensor technologies for cancer cell detection," *Int. J. Opt.*, vol. 2022, pp. 1–10, Sep. 2022.

[52] Z. Li, Y. Cheng, H. Luo, F. Chen, and X. Li, "Dual-band tunable terahertz perfect absorber based on all-dielectric InSb resonator structure for sensing application," *J. Alloys Compounds*, vol. 925, Dec. 2022, Art. no. 166617.

[53] Z. Xu, Y. Wang, J. Chang, and T. J. Cui, "Multiple spoof plasmonically induced transparency for sensing applications," *Phys. Rev. Appl.*, vol. 18, no. 2, Aug. 2022, Art. no. 024035.

[54] D. Wang et al., "Highly sensitive sensing of a magnetic field and temperature based on two open ring channels SPR-PCF," *Opt. Exp.*, vol. 30, no. 21, p. 39055, 2022.

[55] Q. Shangguan et al., "High sensitivity active adjustable graphene absorber for refractive index sensing applications," *Diamond Rel. Mater.*, vol. 128, Oct. 2022, Art. no. 109273.

[56] G. Saxena et al., "CSRR loaded multiband THz MIMO antenna for nano-communications and bio-sensing applications," *Nano Commun. Netw.*, vol. 38, Dec. 2023, Art. no. 100481.

[57] G. Ji et al., "Terahertz virus-sized gold nanogap sensor," *Nanophotonics*, vol. 12, no. 1, pp. 147–154, Jan. 2023.

[58] A. Yadav and A. Gorodetsky, "Biomedical applications of terahertz radiation," in *Advanced Photonics Methods for Biomedical Applications*. Boca Raton, FL, USA: Taylor & Francis, 2023, pp. 67–150.

[59] E. Rafailov and T. Gric, *Advanced Photonics Methods for Biomedical Applications*. Boca Raton, FL, USA: CRC Press, 2023.

[60] A. H. M. Almawgani, M. G. Daher, S. A. Taya, A. T. Hindi, I. Colak, and A. Pal, "Detection of blood cancer using highly sensitive surface plasmon resonance sensor based on MXene 2D nanomaterial," *Diamond Rel. Mater.*, vol. 137, Aug. 2023, Art. no. 110142.

[61] A. R. Elhelw, M. S. S. Ibrahim, A. N. Z. Rashed, A. E.-N.-A. Mohamed, M. F. O. Hameed, and S. S. A. Obayya, "Highly sensitive triple-band THz metamaterial biosensor for cancer cell detection," *IEEE Photon. J.*, vol. 15, no. 6, pp. 1–13, Dec. 2023.

[62] Y. Cheng, Y. Qian, H. Homma, A. A. Fathnan, and H. Wakatsuchi, "Waveform-selective metasurface absorber with a single-patch structure and lumped nonlinear circuit for a higher-order mode," *IEEE Trans. Antennas Propag.*, vol. 71, no. 11, pp. 8677–8691, Nov. 2023.

[63] Y. Cheng, Y. Qian, H. Luo, F. Chen, and Z. Cheng, "Terahertz narrowband perfect metasurface absorber based on micro-ring-shaped GaAs array for enhanced refractive index sensing," *Phys. E, Low-dimensional Syst. Nanostruct.*, vol. 146, Jan. 2023, Art. no. 115527.

[64] Z. Huang et al., "High-resolution metalens imaging polarimetry," *Nano Lett.*, vol. 23, no. 23, pp. 10991–10997, Dec. 2023.

[65] J. Ma et al., "A five-peaks graphene absorber with multiple adjustable and high sensitivity in the far infrared band," *Diamond Rel. Mater.*, vol. 136, Jun. 2023, Art. no. 109960.

[66] W. Zhu et al., "High confidence plasmonic sensor based on photonic crystal fibers with a U-shaped detection channel," *Phys. Chem. Chem. Phys.*, vol. 25, no. 12, pp. 8583–8591, 2023.

[67] M. N. Hamza and M. T. Islam, "Designing an extremely tiny dual-band biosensor based on MTMs in the terahertz region as a perfect absorber for non-melanoma skin cancer diagnostics," *IEEE Access*, vol. 11, pp. 136770–136781, 2023.

[68] S. Li et al., "A polarization-independent fiber-optic SPR sensor," *Sensors*, vol. 18, no. 10, p. 3204, 2018.

[69] M. Abdelsalam, A. M. Mahmoud, and M. A. Swillam, "Polarization independent dielectric metasurface for infrared beam steering applications," *Sci. Rep.*, vol. 9, no. 1, p. 10824, Jul. 2019.

[70] K. Ahmed, B. K. Paul, F. Ahmed, M. A. Jabin, and M. S. Uddin, "Numerical demonstration of triangular shaped photonic crystal fibre-based biosensor in the terahertz range," *IET Optoelectron.*, vol. 15, no. 1, pp. 1–7, Feb. 2021.

[71] M. A. Jabin et al., "Surface plasmon resonance based titanium coated biosensor for cancer cell detection," *IEEE Photon. J.*, vol. 11, no. 4, pp. 1–10, Aug. 2019.

[72] P. Kumar, V. Kumar, and J. S. Roy, "Dodecagonal photonic crystal fibers with negative dispersion and low confinement loss," *Optik*, vol. 144, pp. 363–369, Sep. 2017.

[73] T. Parvin, K. Ahmed, A. M. Alatwi, and A. N. Z. Rashed, "Differential optical absorption spectroscopy-based refractive index sensor for cancer cell detection," *Opt. Rev.*, vol. 28, no. 1, pp. 134–143, Feb. 2021.

[74] P. Sharma, P. Sharan, and P. Deshmukh, "A photonic crystal sensor for analysis and detection of cancer cells," in *Proc. Int. Conf. Pervasive Comput. (ICPC)*, Jan. 2015, pp. 1–5.

[75] M. Gómez-Castaño, J. L. Garcia-Pomar, L. A. Pérez, S. Shanmugathasan, S. Ravaine, and A. Mihi, "Electrodeposited negative index metamaterials with visible and near infrared response," *Adv. Opt. Mater.*, vol. 8, no. 19, Oct. 2020, Art. no. 2000865.

[76] R. Krause et al., "Ultrafast charge separation in bilayer WS_2/graphene heterostructure revealed by time- and angle-resolved photoemission spectroscopy," *Frontiers Phys.*, vol. 9, Apr. 2021, Art. no. 668149.

[77] T. Chen, D. Zhang, F. Huang, Z. Li, and F. Hu, "Design of a terahertz metamaterial sensor based on split ring resonator nested square ring resonator," *Mater. Res. Exp.*, vol. 7, no. 9, Sep. 2020, Art. no. 095802.
[78] S. Asgari, N. Granpayeh, and T. Fabritius, "Controllable terahertz cross-shaped three-dimensional graphene intrinsically chiral metastructure and its biosensing application," *Opt. Commun.*, vol. 474, Nov. 2020, Art. no. 126080.
[79] J. Yang and Y.-S. Lin, "Design of tunable terahertz metamaterial sensor with single- and dual-resonance characteristic," *Nanomaterials*, vol. 11, no. 9, p. 2212, Aug. 2021.
[80] M. Y. Azab, M. F. O. Hameed, A. M. Nasr, and S. S. A. Obayya, "Highly sensitive metamaterial biosensor for cancer early detection," *IEEE Sensors J.*, vol. 21, no. 6, pp. 7748–7755, Mar. 2021.
[81] C. Tan et al., "Cancer diagnosis using terahertz-graphene-metasurface-based biosensor with dual-resonance response," *Nanomaterials*, vol. 12, no. 21, p. 3889, Nov. 2022.
[82] H. Hu, B. Qi, Y. Zhao, X. Zhang, Y. Wang, and X. Huang, "A graphene-based THz metasurface sensor with air-spaced structure," *Frontiers Phys.*, vol. 10, Sep. 2022, Art. no. 990126.
[83] E. Hoseini, A. Mir, and A. Farmani, "Modeling and proposal of a black phosphorus-based nanostructure for detection of avian influenza virus in infrared region," *Opt. Quantum Electron.*, vol. 54, no. 10, p. 609, Oct. 2022.
[84] S. K. Ghosh, A. Chaudhuri, P. Pal, B. Rai, S. Das, and S. Bhattacharyya, "A broadband biosensor using graphene-metasurface based cross-polarization converter," *IEEE Sensors J.*, vol. 22, no. 13, pp. 12820–12828, Jul. 2022.
[85] S. Asgari and T. Fabritius, "Numerical simulation and equivalent circuit model of multi-band terahertz absorber composed of double-sided graphene comb resonator array," *IEEE Access*, vol. 11, pp. 36052–36063, 2023.
[86] L. Liu, W. Liu, and Z. Song, "Ultra-broadband terahertz absorber based on a multilayer graphene metamaterial," *J. Appl. Phys.*, vol. 128, no. 9, pp. 093104-1–093104-6, Sep. 2020, doi: 10.1063/5.0019902.
[87] Y. Wang et al., "Terahertz tunable three band narrowband perfect absorber based on dirac semimetal," *Phys. E, Low-Dimensional Syst. Nanostruct.*, vol. 131, Jul. 2021, Art. no. 114750.
[88] B.-X. Wang, Y. He, P. Lou, and W. Xing, "Design of a dual-band terahertz metamaterial absorber using two identical square patches for sensing application," *Nanosc. Adv.*, vol. 2, no. 2, pp. 763–769, 2020.
[89] S. Zhuang et al., "Graphene-based absorption–transmission multi-functional tunable THz metamaterials," *Micromachines*, vol. 13, no. 8, p. 1239, Aug. 2022.
[90] Z. Chen et al., "Graphene multi-frequency broadband and ultra-broadband terahertz absorber based on surface plasmon resonance," *Electronics*, vol. 12, no. 12, p. 2655, Jun. 2023.
[91] Z. El-Wasif, T. Ismail, and O. Hamdy, "Design and optimization of highly sensitive multi-band terahertz metamaterial biosensor for coronaviruses detection," *Opt. Quantum Electron.*, vol. 55, no. 7, p. 604, Jul. 2023.
[92] Z. Vafapour, W. Troy, and A. Rashidi, "Colon cancer detection by designing and analytical evaluation of a water-based THz metamaterial perfect absorber," *IEEE Sensors J.*, vol. 21, no. 17, pp. 19307–19313, Sep. 2021.
[93] A. S. Saadeldin, M. F. O. Hameed, E. M. A. Elkaramany, and S. S. A. Obayya, "Highly sensitive terahertz metamaterial sensor," *IEEE Sensors J.*, vol. 19, no. 18, pp. 7993–7999, Sep. 2019.
[94] M.-R. Nickpay, M. Danaie, and A. Shahzadi, "Highly sensitive THz refractive index sensor based on folded split-ring metamaterial graphene resonators," *Plasmonics*, vol. 17, no. 1, pp. 237–248, Feb. 2022.

Musa N. Hamza received the B.Sc. degree from the Department of Physics, Faculty of Science and Health, Koya University, Koya, Iraq, in 2015, and the M.Sc. degree from the Department of Medical Physics, College of Medical and Applied Sciences, Charmo University, Chamchamal, Iraq, in 2023.

His research interests include medical physics, the diagnosis of different types of cancer at an early stage, antenna arrays, metamaterials, sensors, and biosensors.

Mohammad Tariqul Islam (Senior Member, IEEE) is currently a Professor with the Department of Electrical, Electronic and Systems Engineering, Universiti Kebangsaan Malaysia (UKM), Bangi, Malaysia, and a Visiting Professor with Kyushu Institute of Technology, Kitakyushu, Japan. He is the author and coauthor of about 600 research journal articles, nearly 250 conference articles, and a few book chapters on various topics related to antennas, metamaterials, and microwave imaging with 25 inventory patents filed. Thus far, his publications have been cited 15 700 times and his H-index is 56 (source: Scopus). His Google Scholar citation is 25 000 and his H-index is 66. He was a recipient of more than 40 research grants from Malaysian Ministry of Science, Technology and Innovation, Ministry of Education, UKM research grant, and international research grants from Japan, Saudi Arabia, and Kuwait. His research interests include communication antenna design, metamaterial, satellite antennas, and microwave imaging.

Dr. Islam has been serving as an Executive Committee Member for IEEE AP/MTT/EMC Malaysia Chapter, from 2019 to 2020, the Chartered Professional Engineer (CEng), a Fellow of IET, U.K., and a Senior Member of IEICE, Japan. He received several International Gold Medal awards, the Best Invention in Telecommunication Award for his research and innovation, and Best Researcher Award at UKM. He was a recipient of the 2018, 2019, and 2020 IEEE AP/MTT/EMC Malaysia Chapter, Excellent Award. He also won the best innovation award and the Best Researcher award by UKM, in different years. He was a recipient of a Publication Award from the Malaysian Space Agency for several years. He has supervised about 50 Ph.D. theses and 30 M.Sc. theses and has mentored more than ten postdocs and Visiting scholars. He has developed the Antenna Measurement Laboratory which includes antenna design and measurement facility till 40 GHz. He was an Associate Editor of *IET Electronics Letter*. He also serves as the Guest Editor for *Sensors* journal, *Nanomaterials*, and an Associate Editor for IEEE ACCESS.